Effects of thermodynamics parameters on mass transfer of volatile pollutants at air-water interface

Li-ping Chen [a],*, Kai-yun Xuan [a], Bin Zhou [a], Guang-fa Deng [b]

[a] *College of Urban Construction, Nanjing University of Technology, Nanjing 210009, PR China*
[b] *Jiangsu Frontier Electric Technology Co., Ltd., Nanjing 211102, PR China*

Abstract

A transient three-dimensional coupling model based on the compressible volume of fluid (VOF) method was developed to simulate the transport of volatile pollutants at the air-water interface. VOF is a numerical technique for locating and tracking the free surface of water flow. The relationships between Henry's constant, thermodynamics parameters, and the enlarged topological index were proposed for nonstandard conditions. A series of experiments and numerical simulations were performed to study the transport of benzene and carbinol. The simulation results agreed with the experimental results. Temperature had no effect on mass transfer of pollutants with low transfer free energy and high Henry's constant. The temporal and spatial distribution of pollutants with high transfer free energy and low Henry's constant was affected by temperature. The total enthalpy and total transfer free energy increased significantly with temperature, with significant fluctuations at low temperatures. The total enthalpy and total transfer free energy increased steadily without fluctuation at high temperatures.
© 2015 Hohai University. Production and hosting by Elsevier B.V. This is an open access article under the CC BY-NC-ND license (http://creativecommons.org/licenses/by-nc-nd/4.0/).

Keywords: Henry's constant; Mass transfer at interface; Thermodynamics parameters; Topological index; Volatile pollutants

1. Introduction

Accurately predicting the temporal and spatial distribution of volatile pollutants in water and air after leakage can provide an important insight for health evaluation of hydrosphere ecosystems. However, mass transfer of volatile pollutants at the air-water interface is a complex process and we do not yet have a deep and accurate understanding of its mechanisms and factors (Jähne and Haubecker, 1998; Bade, 2009; Wang et al., 2011). This affects the prediction results of the temporal and spatial distribution of volatile pollutants. Thus, it is necessary to reach a better understanding of mass transfer of volatile pollutants at the air-water interface.

In computational fluid dynamics, the volume of fluid (VOF) method is a numerical technique for locating and tracking the air-water interface (Larmaei and Mahdi, 2010). A transient three-dimensional coupling transport model based on the compressive VOF method was used to simulate mass transfer at the air-water interface (Chen and Jiang, 2010). Henry's constant is an important parameter in a coupling transport model for volatile pollutants. It relates not only to the thermodynamics parameters, such as the transfer free energy and the standard enthalpy, but also to the molecular structure of pollutants (Cheng et al., 2004; Amelia et al., 2011; Duran et al., 2010). Quantitative structure-activity/property relationships (QSAR/QSPR) represent an attempt to correlate activities or properties with structural descriptors of compounds. There are many methods for quantifying molecular structures, of which the topological index is the most popular since it can be obtained directly from molecular structures and rapidly

computed for large numbers of molecules. The first reported use of a topological index in chemistry was by Wiener in his study of paraffin boiling points (Wiener, 1947). Degeneracy and low discriminating power have been the two shortcomings of Wiener's index, resulting in ambiguity and uniqueness in its properties. This is one major reason that Wiener's index has not seen widespread use in the QSAR/QSPR community (Bajaj et al., 2004). The enlarged topological index of distance matrix W^* has been defined to forecast Henry's constants of some alkylbenzene and alcohol compounds in standard conditions (Yang et al., 2004). At present, the relationship between Henry's constant and the molecular structure of pollutants in nonstandard conditions has not been established. Mathematical models have been developed to describe the relationships between Henry's constant, thermodynamics parameters, and W^* in nonstandard conditions in this study.

Thermodynamics parameters such as the transfer free energy and the standard enthalpy have been used for volatilization study in recent years. The transfer free energy and the standard enthalpy are defined for per mole of pollutants and they are independent of time. However, mass transfer at the air-water interface in sudden water pollution relates to time. Thus, the transfer free energy and the standard enthalpy cannot be used as effective thermodynamic parameters in sudden water pollution. Total transfer free energy and total enthalpy were defined to analyze the changes of thermodynamics parameters with time at different temperatures. The total transfer free energy and total enthalpy for mass transfer at the air-water interface are discussed below.

2. Model development

2.1. Mathematical equations for transportation

The equations for compressive VOF are as follows (Chen and Jiang, 2010):

$$\frac{\partial \rho}{\partial t} + \frac{\partial (\rho u_i)}{\partial x_i} = 0 \tag{1}$$

$$\frac{\partial (\rho u_j)}{\partial t} + \frac{\partial (\rho u_j u_i)}{\partial x_i} = \frac{\partial}{\partial x_j}\left(\eta_t \frac{\partial u_j}{\partial x_i}\right) - \frac{\partial p}{\partial x_j} + \rho f_j \tag{2}$$

$$\frac{\partial \alpha}{\partial t} + \frac{\partial (u_i \alpha)}{\partial x_i} - \frac{\partial}{\partial x_i}\left[\frac{(u_{Gi} - u_{Li})(1-\alpha)\alpha \rho_G}{\rho}\right] = 0 \tag{3}$$

where ρ and ρ_G are the densities of the fluid in the computational cell and air, respectively, in kg/m³; t is time, in s; the subscripts i and j are equal to 1, 2, or 3, representing the three directions in the Cartesian coordinate system; u, u_L, and u_G are the velocities of the fluid in the computational cell, water, and air, respectively, in m/s; η_t is the turbulent dynamic viscosity, in m²/s, which can be calculated with the realizable k-ε model; f is the body force, in m/s²; p is the pressure, in Pa; and α is the water volumetric fraction of the computational cell.

The air-water coupling transport model for volatile pollutants is written as follows (Chen and Jiang, 2010):

$$\frac{\partial C}{\partial t} + \frac{\partial (u_i C)}{\partial x_i} + \frac{\partial}{\partial x_i}\left[(u_{Gi} - u_{Li})\alpha(1-\alpha)\frac{H_{aw}-1}{\alpha+(1-\alpha)H_{aw}}C\right] = \frac{\partial^2}{\partial x_i \partial x_i}\left[\frac{E_i \alpha + (1-\alpha)H_{aw}D}{\alpha+(1-\alpha)H_{aw}}C\right] \tag{4}$$

where C is the total concentration of pollutants in the computational cell, in kg/L; H_{aw} is Henry's constant; and D and E_i are the turbulent mass diffusivities in air and water, respectively, in m²/s.

2.2. Henry's constant and thermodynamics parameters

The driving force of volatile pollutants' transportation is the difference in chemical potential related to activity coefficients. Mass transfer at the air-water interface is at instantaneous equilibrium. The equilibrium constant is called Henry's constant (Schwarzenbach et al., 2003):

$$H_{aw} = \exp\left(-\frac{RT \ln \gamma_a - RT \ln \gamma_w}{RT}\right) = \exp\left(-\frac{\Delta_{12}G}{RT}\right) \tag{5}$$

where γ_a and γ_w are the activity coefficients of volatile pollutants in air and water, respectively; $\Delta_{12}G$ is the transfer free energy, in J/mol; R is the gas constant, which is 8.314 J/(mol·K); and T is the Kelvin temperature.

Taking the derivative of Eq. (5) with respect to temperature and using the Gibbs-Helmholtz equation (Lucia and Henley, 2013) yield:

$$\frac{d(\ln H_{aw})}{dT} = -\frac{1}{R}\frac{d(\Delta_{12}G/T)}{dT} = \frac{1}{R}\frac{\Delta_{12}H}{T^2} \tag{6}$$

where $\Delta_{12}H$ is the standard enthalpy, in J/mol. It is considered constant over a small temperature range. Henry's constant in nonstandard conditions is obtained from Eq. (6):

$$\ln H_{aw} = -\frac{\Delta_{12}H}{R}\left(\frac{1}{T} - \frac{1}{T_0}\right) + \ln H_0 \tag{7}$$

where H_0 is Henry's constant in standard conditions with $T_0 = 298$ K.

Henry's constant relates not only to the thermodynamics parameters but also to the molecular structure of pollutants. There are many methods of quantifying the molecular structure, of which the topological index is the most popular since it can be obtained directly from molecular structures and rapidly computed for large numbers of molecules. The enlarged topological index of distance matrix W^* was defined as $W^* = MSI$, where $M = (m_1, m_2, \cdots, m_n)$, $S = (S_{kj})_{n \times n}$, $I = (I_1, I_2, \cdots, I_n)^T$, m_k is the number of bonded electrons, I_k is electronegativity, $S_{kj} = 1/R_{kj}$, and R_{kj} is the sum of the bond length from k to j. The linear relationships between $\ln H_0$ and $W^{*0.5}$ of alkylbenzene, alcohol, aldehyde, and hydrocarbon are listed in Table 1 (Yang et al., 2004).

Table 1
Linear relationships between $\ln H_0$ and $W^{*0.5}$ for different compounds.

Compound	Relationships between $\ln H_0$ and $W^{*0.5}$
Alkylbenzene	$\ln H_0 = 0.125\,0W^{*0.5} - 2.086$
Alcohol	$\ln H_0 = 0.053\,6W^{*0.5} - 8.593$
Aldehyde	$\ln H_0 = 0.046\,5W^{*0.5} - 6.327$
Hydrocarbon	$\ln H_0 = 0.220\,6W^{*0.5} - 2.948$

Henry's constant in nonstandard conditions is written as follows:

$$\ln H_{aw} = -\frac{\Delta_{12}H}{R}\left(\frac{1}{T} - \frac{1}{T_0}\right) + aW^{*0.5} + b \tag{8}$$

where a and b are coefficients.

Using Eq. (5) and Eq. (8) yields the equation for the transfer free energy:

$$\Delta_{12}G = \Delta_{12}H\left(1 - \frac{T}{T_0}\right) - RT\left(aW^{*0.5} + b\right) \tag{9}$$

2.3. Thermodynamics properties of benzene and carbinol

In order to examine the effect of thermodynamics parameters on mass transfer at the air-water interface, benzene and carbinol were selected as pollutants. The enlarged topological indexes of the distance matrix W^* of benzene and carbinol are 24.370 and 9.286, respectively. In standard conditions, the standard enthalpies $\Delta_{12}H$ of benzene and carbinol

are 30 kJ/mol and 45 kJ/mol, respectively (Schwarzenbach et al., 2003). Fig. 1 shows the transfer free energy and Henry's constants of benzene and carbinol as functions of temperature.

The transfer free energy $\Delta_{12}G$ of benzene and carbinol decreases slightly with temperature. At the same temperature, the $\Delta_{12}G$ of benzene is only 17.2% that of carbinol. The Henry's constant H_{aw} of benzene rises significantly with temperature, while temperature has no effect on the Henry's constant of carbinol.

3. Experiments and numerical simulations

3.1. Experimental setup

A series of experiments and numerical simulations were performed in a straight flume with a rectangular shape. The experimental facility and the coordinate system are shown in Fig. 2. The flume was 14.0 m long, 0.4 m wide, and 0.4 m deep, and had a 3/700 bed slope (Chen et al., 2013). The water depth was 0.1 m. Flow was in the x direction, and the flume width was in the y direction. The z direction was upward and the bottom of the flume was at $z = 0$. The origin of the coordinates was in the side wall of the flume. The average velocities of water and air were 0.2 m/s and 1.2 m/s, respectively. A pollutant solution of 50 mL with a concentration of 2 g/L was instantaneously released into the flume. The release point was at $x = 1.25$ m, $y = 0.2$ m, and $z = 0.1$ m. Gas chromatography was used to measure the concentrations of benzene and carbinol in air.
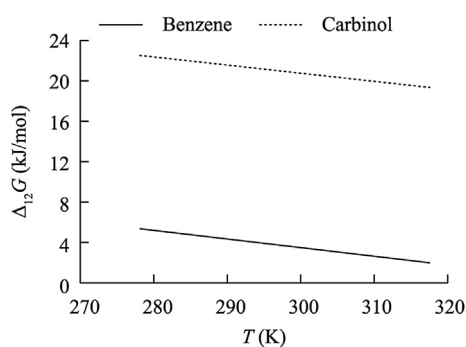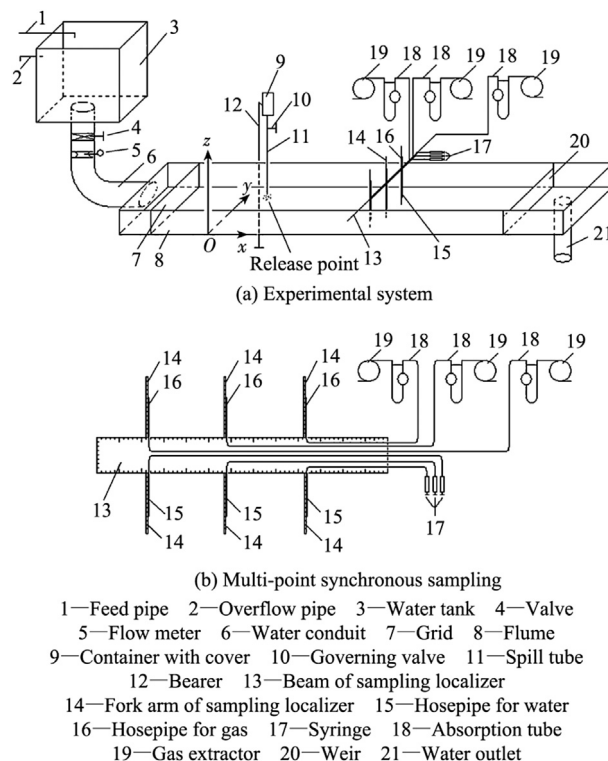

(a) Transfer free energy
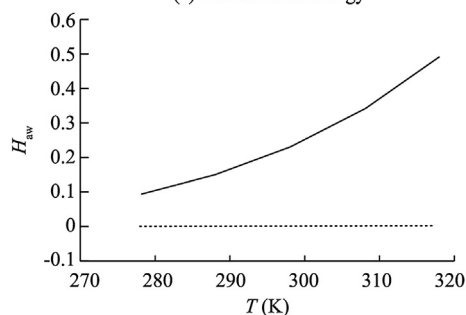
(b) Henry's constant

Fig. 1. Transfer free energy and Henry's constant as functions of temperature.

(a) Experimental system

(b) Multi-point synchronous sampling

1—Feed pipe 2—Overflow pipe 3—Water tank 4—Valve
5—Flow meter 6—Water conduit 7—Grid 8—Flume
9—Container with cover 10—Governing valve 11—Spill tube
12—Bearer 13—Beam of sampling localizer
14—Fork arm of sampling localizer 15—Hosepipe for water
16—Hosepipe for gas 17—Syringe 18—Absorption tube
19—Gas extractor 20—Weir 21—Water outlet

Fig. 2. Experimental facility.

3.2. Numerical methods

3.2.1. Computational zones and boundary conditions

The computational zones shown in Fig. 3 are composed of the flume and air zone. There was no pollutant at the inlet. The flow at the outlet was fully developed. The widely accepted finite volume method (FVM) was applied during model formulation. The pressure-implicit with splitting of operators (PISO) procedure was used for pressure-velocity coupling in calculations (Issa, 1986). The Crank-Nicholson method was used for temporal discretization. The second-order accurate smooth transition differencing scheme (STDS) was used to discretize the convection terms (Chen et al., 2013). The alternating direction implicit (ADI) and tridiagonal matrix algorithm (TDMA) methods were combined to solve the algebraic equations. The realizable k-ε model was used for turbulent flow calculation. The values of k and ε at inlets were given by empirical formulas $k = 0.003\,75u_{in}^2$ and $\varepsilon = k^{1.5}/(0.42D_e)$, respectively, where u_{in} is the velocity at the inlet and D_e is the water depth. The flow parameters at the inlet are listed in Table 2.

3.2.2. Grid independence

The computational zone in the flume was $14 \text{ m} \times 0.4 \text{ m} \times 0.4 \text{ m}$. A computational zone in the air was $14 \text{ m} \times 6.4 \text{ m} 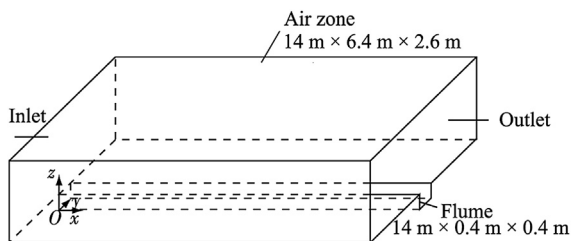\times 2.6 \text{ m}$. A grid system of 188 800 cells were used according to the results of grid independence study from Chen et al. (2013).

4. Results and discussion

4.1. Comparison of concentration

Fig. 4 shows the concentration of pollutants along the flume as functions of time at 298 K, where C_0 is the initial concentration of carbinol or benzene, with a value of 2 g/L. The area with higher concentration of carbinol in water is larger than that of benzene at the same time, and this phenomenon is more pronounced after 3 s. The space occupied by benzene in air is larger than that occupied by carbinol. The diffusion height of benzene in the air is higher than that of carbinol because benzene has a higher H_{aw}. The C/C_0 contours of carbinol in air tend downstream. It is easy for carbinol to be transported downstream at an air speed of 1.2 m/s because of the lower degree of volatilization. However, the air speed has a lesser influence on benzene because there is so much benzene in the air.

Fig. 5(a) shows the variation of C/C_0 with time at a point of $x = 1.75$ m, $y = 0.20$ m, and $z = 0.13$ m, and at a temperature of 308 K. The C/C_0 of benzene reaches the peak and then drops quickly, whereas the C/C_0 of carbinol changes slowly with time. The C/C_0 of carbinol is lower than that of benzene at the start of release due to the higher $\Delta_{12}G$ and lower H_{aw}. Fig. 5(a) means that volatilization of the pollutants with the higher $\Delta_{12}G$ and lower H_{aw} is weak near the release point. Fig. 5(b) shows that the peak C/C_0 of benzene does not increase with temperature, although the H_{aw} of benzene does. The peak C/C_0 of benzene at 318 K is lower than that at 308 K because the $\Delta_{12}G$ of benzene decreases with temperature, and the benzene covering on the water surface restrains volatilization. However, the peak C/C_0 of carbinol increases slightly with temperature.

Fig. 6(a) shows the variation of C/C_0 with time at a point of $x = 2.05$ m, $y = 0.20$ m, and $z = 0.13$ m, and at a temperature of 308 K. This sampling point is far from the release site. The concentration difference between benzene and carbinol in Fig. 6(a) is much lower than that in Fig. 5(a). The reason is that much benzene in air has been transported with air flow. Fig. 6(b) shows that the peak C/C_0 of carbinol at $x = 2.05$ m, $y = 0.20$ m, and $z = 0.13$ m increases significantly with

Fig. 3. Computational zones.

Table 2
Parameters at inlet.

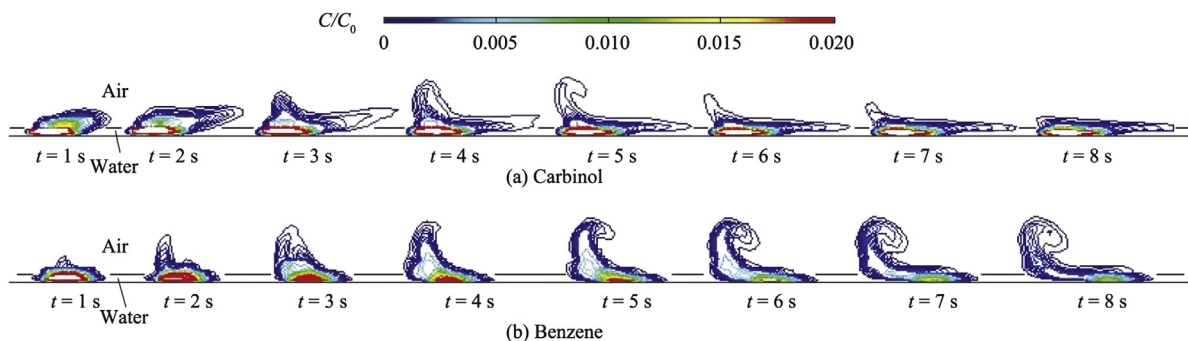| Fluid	Velocity (m/s)	k (m²/s²)	ε (m²/s³)
Water	0.2	1.5×10^{-4}	4.4×10^{-5}
Air	1.2	5.4×10^{-3}	2.1×10^{-4}

Fig. 4. Concentration distribution of pollutants along flume axis at 298 K.
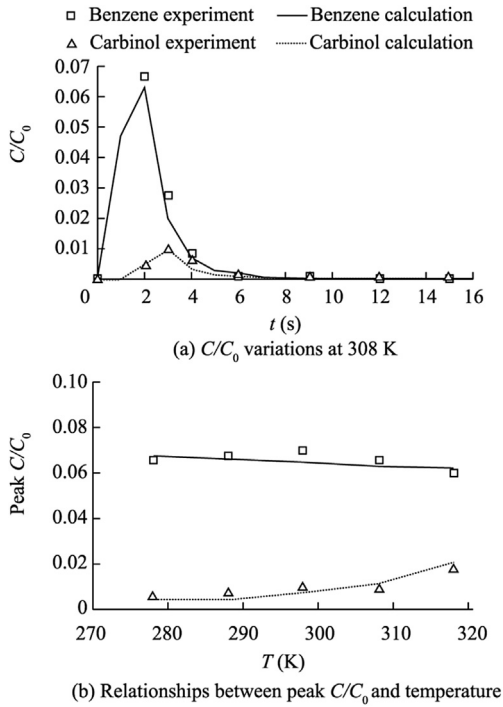
Fig. 5. Concentration distribution of pollutants at point of $x = 1.75$ m, $y = 0.20$ m, and $z = 0.13$ m.

temperature. The peak C/C_0 of carbinol is higher than that of benzene at 318 K. Fig. 6(b) means that volatilization of the pollutants with the higher $\Delta_{12}G$ and lower H_{aw} cannot be ignored during later release period at higher temperatures.
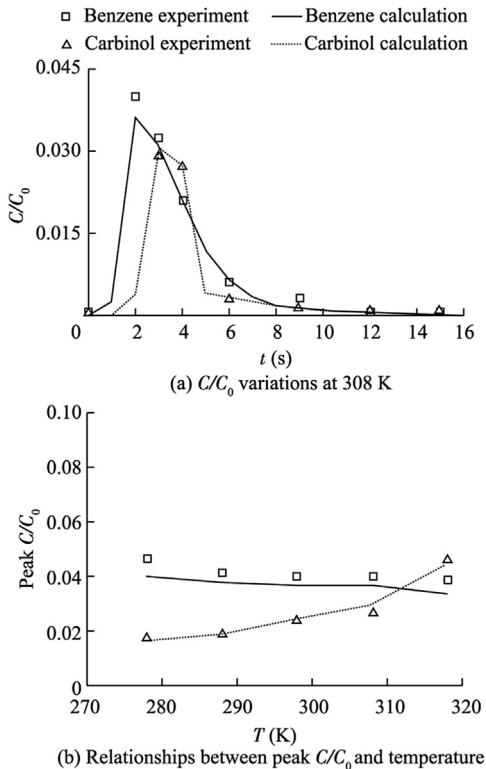
4.2. Changes of total enthalpy and total transfer free energy at different temperatures

Mass transfer at the air-water interface relates to time in sudden leakage. However, $\Delta_{12}H$ and $\Delta_{12}G$ are independent of time. They cannot be used as parameters reflecting the thermodynamics variations during the process of mass transfer. The total enthalpy $\Delta_{12}H_T$ is defined as the product of the amount of volatility and $\Delta_{12}H$. The total transfer free energy $\Delta_{12}G_T$ is defined as the product of the amount of volatility and $\Delta_{12}G$. $\Delta_{12}H_T$ and $\Delta_{12}G_T$ are thermodynamics parameters related to time. Though $\Delta_{12}H$ is constant in the range of environmental temperature, $\Delta_{12}H_T$ changes significantly with temperature. Fig. 7 shows the variations of $\Delta_{12}H_T$ and $\Delta_{12}G_T$ with time for carbinol at different temperatures. The change patterns of $\Delta_{12}H_T$ and $\Delta_{12}G_T$ are consistent with each other. $\Delta_{12}H_T$ and $\Delta_{12}G_T$ increase linearly during the initial leakage at 0−3 s. Then, $\Delta_{12}H_T$ and $\Delta_{12}G_T$ increase slowly with time at higher temperatures. $\Delta_{12}H_T$ and $\Delta_{12}G_T$ fluctuate significantly at 278 K and 288 K over 4−16 s. Pollutants absorbing $\Delta_{12}G$ from the surroundings can be transferred from water to air. It is difficult for the pollutants to absorb energy from the surroundings at lower temperatures. Thus, the amount of volatility is low and the gaseous pollutants with lower chemical potential return to water easily, resulting in the significant fluctuations of $\Delta_{12}H_T$ and $\Delta_{12}G_T$ at lower temperatures. At higher temperatures, pollutants absorbing $\Delta_{12}G$ have higher chemical potential. The gaseous pollutants with higher chemical potential are transported easily in air and cannot

Fig. 6. Concentration distribution of pollutants at point of $x = 2.05$ m, $y = 0.20$ m, and $z = 0.13$ m.
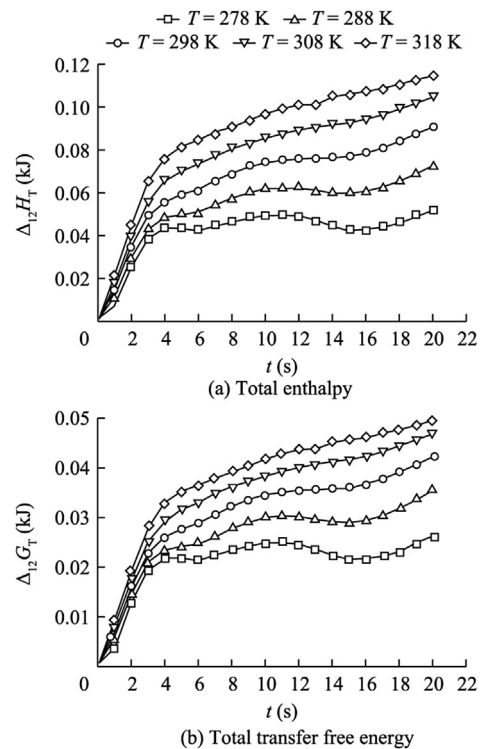

Fig. 7. Variations of total enthalpy and total transfer free energy of carbinol with time.

return to water. Thus, $\Delta_{12}H_T$ and $\Delta_{12}G_T$ increase steadily without fluctuation at higher temperatures.

5. Conclusions

(1) The compressive VOF method was used to develop a coupling transport model for volatile pollutants. Mathematical models were developed to describe the relationships between Henry's constant, thermodynamics parameters, and the enlarged topological index of distance matrix W^* in nonstandard conditions. Henry's constant increases with W^* and the transfer free energy decreases with W^*.

(2) Experiments were carried out in a flume, and benzene and carbinol were selected as pollutants. For benzene with low transfer free energy and high Henry's constant, the gaseous concentration is very large near the release site at the start of release. After a few seconds, benzene covering on the water surface restrains volatilization due to the coupling action. Temperature has no effect on mass transfer at the air-water interface for benzene. For carbinol with high transfer free energy and a low Henry's constant, the gaseous concentration cannot restrain volatilization. The temporal and spatial distribution of carbinol is affected by temperature.

(3) The standard enthalpy is constant in the range of environmental temperature. The total enthalpy and total transfer free energy increase significantly with temperature. Their fluctuations are significant at low temperatures. However, they increase steadily without fluctuation at high temperatures.

References

Amelia, T.G., Julia, M.V., Antonio, M.R., David, J.M., 2011. Physicochemical properties and digestibility of emulsified lipids in simulated intestinal fluids: Influence of interfacial characteristics. Soft Matter 7(13), 6167−6177. http://dx.doi.org/10.1039/C1SM05322A.

Bade, D.L., 2009. Gas exchange at the air-water interface. Encycl. Inland Waters 3, 70−78. http://dx.doi.org/10.1016/B978-012370626-3.00213-1.

Bajaj, S., Sambi, S.S., Mada, A.K., 2004. Predicting anti-HIV activity of phenethylthiazolethiourea (PETT) analogs: Computational approach using Wiener's topochemical index. J. Mol. Struct. (Theochem) 684(1−3), 197−203. http://dx.doi.org/10.1016/j.theochem.2004.01.052.

Chen, L.P., Jiang, J.C., 2010. Coupling diffusion simulation of volatile pollutant in the water and air. J. Civ. Archit. Environ. Eng. 32(5), 102−108. http://dx.doi.org/10.11835/j.issn.1674-4764.2010.05.019.

Chen, L.P., Cheng, J.J., Deng, G.F., 2013. Anisotropic diffusion of volatile pollutants at air-water interface. Water Sci. Eng. 6(2), 153−163. http://dx.doi.org/10.3882/j.issn.1674-2370.2013.02.004.

Cheng, W.H., Chou, M.S., Perng, C.H., Chu, F.S., 2004. Determining the equilibrium partitioning coefficients of volatile organic compounds at an air-water interface. Chemosphere 54(7), 935−942. http://dx.doi.org/10.1016/j.chemosphere.2003.08.038.

Duran, T.R., Camredon, M., Valorso, R., 2010. Structure-activity relationships to estimate the effective Henry's law constants of organics of atmospheric interest. Atmos. Chem. Phys. 10, 7643−7654. http://dx.doi.org/10.5194/acp-10-7643-2010.

Issa, R.I., 1986. Solution of the implicitly discretised fluid flow equations by operator-splitting. J. Comput. Phys. 62, 40−65. http://dx.doi.org/10.1016/0021-9991(86)90099-9.

Jähne, B., Haubecker, H., 1998. Air-water gas exchange. Annu. Rev. Fluid Mech. 30, 443−468. http://dx.doi.org/10.1146/annurev.fluid.30.1.443.

Larmaei, M.M., Mahdi, T.F., 2010. Simulation of shallow water waves using VOF method. J. Hydro-Environ. Res. 3(4), 208−214. http://dx.doi.org/10.1016/j.jher.2009.10.010.

Lucia, A., Henley, H., 2013. Thermodynamic consistency of the multi-scale Gibbs-Helmholtz constrained equation of state. Chem. Eng. Res. Des. 91(9), 1748−1759. http://dx.doi.org/10.1016/j.cherd.2013.03.009.

Schwarzenbach, R.P., Gschwend, P.M., Imboden, D.M., 2003. Environmental Organic Chemistry. John Wiley & Sons Inc., Hoboken.

Wang, Y.T., Hodas, N.O., Jung, Y., Marcus, R.A., 2011. Microscopic structure and dynamics of air/water interface by computer simulations-comparison with sum-frequency generation experiments. Phys. Chem. Chem. Phys. 13(12), 5388−5393. http://dx.doi.org/10.1039/c0cp02745f.

Wiener, H., 1947. Structural determination of paraffin boiling points. J. Am. Chem. Soc. 69(1), 17−20. http://dx.doi.org/10.1021/ja01193a005.

Yang, F., Wang, Z.D., Huang, Y.P., 2004. Modification of the Wiener index 4. J. Comput. Chem. 25(6), 881−887. http://dx.doi.org/10.1002/jcc.20016.